doi:10.1006/jmbi.2001.4790 available online at http://www.idealibrary.com on IDEAL® *J. Mol. Biol.* (2001) **310**, 895–906

JMB

Solution Structure of the Tumor Necrosis Factor Receptor-1 Death Domain

Steven F. Sukits[1], Lih-Ling Lin[2], Sang Hsu[2], Karl Malakian[1] Robert Powers[1] and Guang-Yi Xu[1]*

[1]*Department of Biological Chemistry and*

[2]*Department of Musculoskeletal Science, Wyeth Research, 87 Cambridge Park Drive Cambridge, MA 02140, USA*

**Corresponding author*

Tumor necrosis factor receptor-1 death domain (TNFR-1 DD) is the intracellular functional domain responsible for the receptor signaling activities. The solution structure of the R347K mutant of TNFR-1 DD was solved by NMR spectroscopy. A total of 20 structures were calculated by means of hybrid distance geometry-simulated annealing using a total of 1167 distance constraints and 117 torsion angle constraints. The atomic rms distribution about the mean coordinate positions for the 20 structures for residues composing the secondary structure region is 0.40 Å for the backbone atoms and 1.09 Å for all atoms. The structure consists of six antiparallel α-helices arranged in a similar fashion to the other members of the death domain superfamily. The secondary structure and three-dimensional structure of R347K TNFR1-DD are very similar to the secondary structure and deduced topology of the R347A TNFR1-DD mutant. Mutagenesis studies identified critical residues located in α2 and part of α3 and α4 that are crucial for self-interaction and interaction with TRADD. Structural superposition with previously solved proteins in the death domain superfamily reveals that the major differences between the structures reside in α2, α3, and α4. Interestingly, these regions correspond to the binding sites of TNFR1-DD, providing a structural basis for the specificity of death domain interactions and its subsequent signaling event.

Keywords: TNFR-1; death domain; structure; NMR; apoptosis

Introduction

Activation of the tumor necrosis factor receptor-1 (TNFR-1) by the ligand TNF initiates two major intracellular signaling pathways that lead to the activation of the transcription factor NFκB[1] and the induction of cell death.[2,3] TNFR-1 trimerizes upon binding to the TNF trimer inducing association of its intracellular death domain (DD).[4] The trimerization of TNFR-1 allows for the recruitment of an adaptor protein named TNFR-associated death domain protein (TRADD) through a death domain/death domain interaction. TRADD[5] recruits the signaling molecules TNFR-associated factor-2 (TRAF-2)[6] through interactions with the N-terminal domain, Fas-associated death domain protein (FADD) through death domain interactions,[6] and the receptor interacting protein (RIP) through death domain interactions[7] to form the TNFR-1 signaling complex.

The death domain is a protein interaction motif involved in homo- and hetero-association[8] that was originally described as a region of similarity within the intracellular portions of the TNFR-1 and Fas/Apo1 that is essential for the transduction of cytotoxic signals.[9,10] Structural studies of death domains have been problematic due to the propensity to self-associate and form large molecular mass aggregates at physiological pH. This is also the case for the death effector domains (DED) and the caspase recruiting domains (CARD), which are structurally related to the death domains. Therefore, structural studies of the death domain super-

Abbreviations used: TNFR-1, tumor necrosis factor receptor-1; DD, death domain; TRADD, TNFR-associated death domain protein; TRAF-2, TNFR-associated factor-2; FADD, Fas associated death domain protein; RIP, receptor interacting protein; DED, death effector domains; CARD, Caspase recruiting domains; SODD, silencer of death domains; HSQC, heteronuclear single quantum coherence; NOE, nuclear Overhauser enhancement.

E-mail address of the corresponding author: gxu@genetics.com

0022-2836/01/040895–12 $35.00/0

family of proteins requires relatively low ($\leqslant 4$) or high ($\geqslant 8$) pH to minimize the natural tendency for the proteins to self-aggregate. To date, a total of four unique death domain structures have been reported, Fas DD,[11] p75 neurotrophin,[12] FADD DD[13,14] and a complex structure of the Tube DD with the Pelle DD.[15] In addition, one death effector domain structure (FADD DED)[16] and four CARD domain structures, RAIDD CARD,[17] APAF-1 CARD,[18,19] and the complex between APAF-1 CARD and procaspase-9[19] have been solved. The structures all have the same general fold consisting of a core of six α-helices arranged in an antiparallel fashion, but the lengths and orientations of the α-helices are slightly different when comparing one structure to another. Here, we report the solution structure of the mutant R347K TNFR-1 DD. The structure of the R347K TNFR-1 DD consists of six antiparallel α-helices with a topology similar to the previously reported structures of proteins in the death domain superfamily.

Results

Structure determination

Historically, death domains have posed problems for NMR studies at physiological pH due to their tendency to self-associate and form large molecular mass aggregates. A potential solution to the self-association of death domain proteins is the utilization of relatively low ($\leqslant 4$) or high ($\geqslant 8$) pH. Also, single-point mutations have been shown to disrupt self-association and make structural studies amenable, which was the case for the FADD DED solution structure.[16] The current analysis of the TNFR-1 DD solution structure has relied on the R347K single-point mutation and low pH to eliminate aggregation of the protein.

The wild-type TNFR-1 DD was very insoluble and not amenable to NMR structural studies over a wide pH range (4-10); therefore, mutant proteins were made to improve the solubility and stability of the protein. R347 was chosen as the site of mutation because it is one of the conserved residues that mediates both cytotoxicity[9] and binding ability of TNFR-1 DD.[20] As previously described, the solubility and stability of the R347A mutant at high pH (8.8) allowed for secondary structure determination and an insight into the topological fold of the protein.[20] Due to severe broadening of the amide proton peaks because of rapid exchange with water at high pH (8.8), complete assignment and structure determination of the protein was hindered. Nevertheless, it was demonstrated that the majority of R347A TNFR-1 DD forms α-helices, where the amide proton exchange is reduced by hydrogen bond formation. This allowed for the observation of backbone chemical shifts and the determination of sequential assignments in the α-helical regions using triple resonance experiments. The mutation of R347 to lysine allowed for NMR studies to be performed at low pH (4.0) where the exchange with water is reduced. At pH 4.0, the solubility of the R347K TNFR-1 DD mutant was ~1 mM and the protein ran predominantly as a monomer on a gel-filtration column. Additionally, the protein appears folded by analysis of an HSQC correlation experiment collected on ^{15}N-labeled protein.

NMR-derived data that summarize the secondary structural elements of R347K TNFR-1 DD is illustrated in Figure 1. Medium-range NOEs: $d_{NN}(i,i+2)$, $d_{\alpha N}(i,i+3)$, $d_{\alpha N}(i,i+4)$, and $d_{\alpha\beta}(i,i+3)$ along with C^{α} and C^{β} secondary chemical shifts identify the six α-helical regions of the protein. Additionally, the experimentally measured coupling constants ($^3J_{HNH\alpha}$) and the hydrogen-deuterium exchange data correlate well with five of the α-helices. The amide protons located in α3 exchange quickly with ^2H_2O relative to those located in the other α-helices in the structure. The approximate lengths of the α-helices are from residues A328 to N336 (α1), W342 to L349 (α2), D353 to L361 (α3), L367 to R380 (α4), L389 to D398 (α5), and G403 to L412 (α6). The N and C-terminal regions are unstructured and both exhibit multiple peptidyl-prolyl isomers due to the presence of six proline residues. The N and C-terminal regions were not included in the structure calculations. The solution structure of R347K TNFR-1 DD, which encompasses residues P327-C413, was determined from a total of 1167 distance constraints comprising 264 intra-residue, 279 sequential, 247 medium-range, 295 long-range distance constraints, and 82 distance constraints from 41 backbone hydrogen bonds. Additionally, 117 torsion angle constraints comprised of 56 ϕ, 56 ψ, one χ_1, and four χ_2 dihedral constraints, and 81 C^{α} and 77 C^{β} chemical shift constraints were used for the structure calculations. Figure 2(a) presents a ribbon diagram of the C^{α} trace of the average minimized structure of R347K TNFR-1 DD. Figure 2(b) presents a stereoview of an overlay of the C^{α} trace for the best 20 simulated annealing structures for the R347K TNFR-1 DD. The final ensemble of 20 structures contained no distance constraint violation greater than 0.25 Å and no torsion angle constraint violation greater than 3°. The solution structures are well defined, as evident by the atomic rmsd of the 20 simulated annealing structures about the mean coordinate positions, where the backbone of the α-helical regions and all atoms in the α-helical region is 0.40 Å and 1.09 Å, respectively. The R347K TNFR-1 DD solution structure is consistent with a good-quality structure based on PROCHECK and Ramachandran analysis.[21,22] The Ramachandran plot of the minimized average structure shows that 93.6% of the residues are in the most-favored region and 6.4% are in the additionally allowed region. PROCHECK analysis indicates an overall *G*-factor of 0.26 and only three bad contacts. A summary of the structural statistics for the 20 simulated annealing structures of R347K TNFR-1 DD is provided in Table 1.

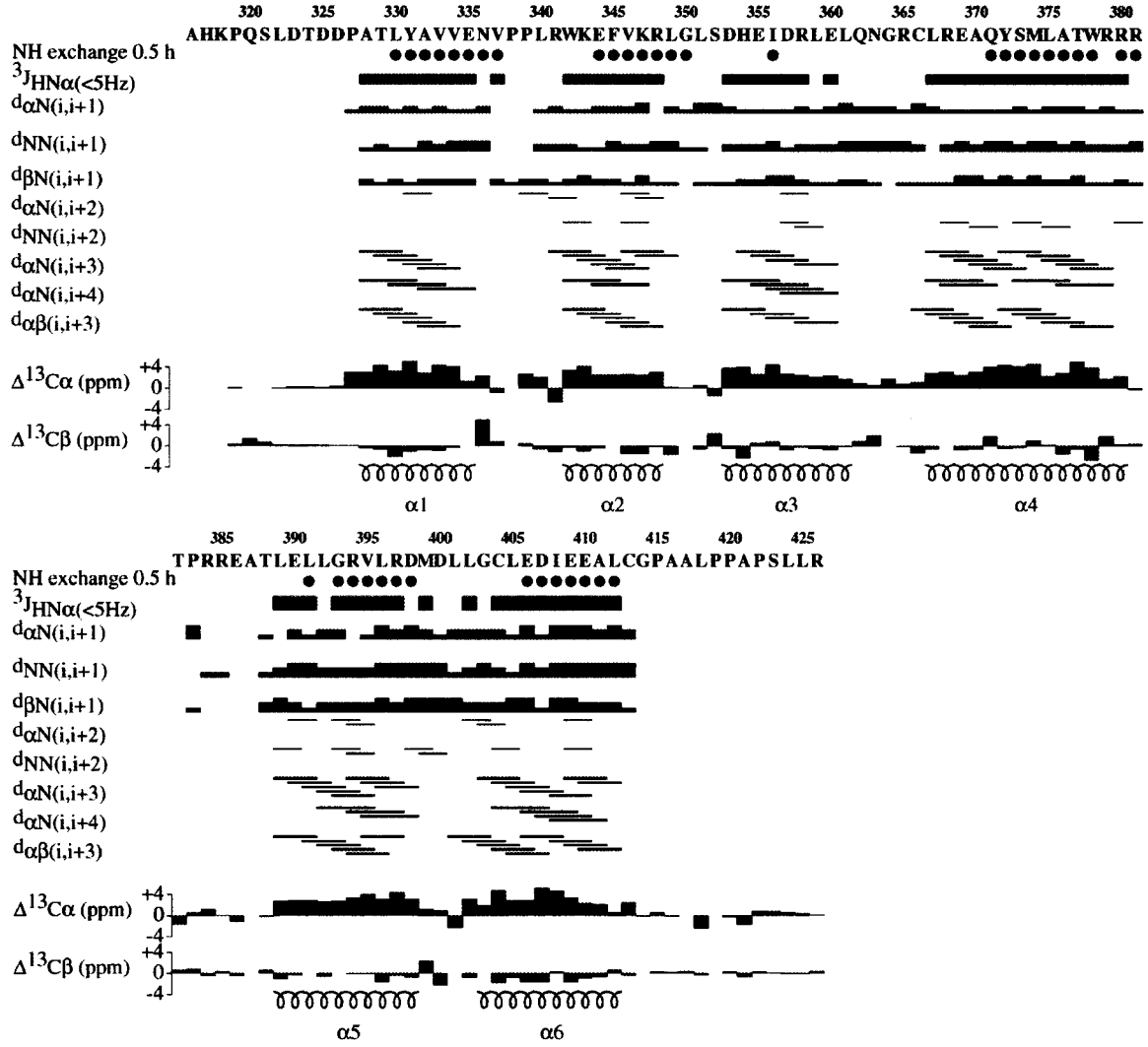

Figure 1. Summary of ^{1}H-^{2}H exchange, $^{3}J_{HNH\alpha}$ scalar coupling information, sequential NOEs ($d_{\alpha N}$, d_{NN}, $d_{\beta N}$), medium-range NOEs ($d_{NN}(i,i+2)$, $d_{\alpha N}(i,i+3)$), $d_{\alpha N}(i,i+4)$, $d_{\alpha\beta}(i,i+3)$), and the $\Delta^{13}C^{\alpha}$ and $\Delta^{13}C^{\beta}$ chemical shift index. Amide protons that did not exchange with $^{2}H_2O$ within 30 minutes are designated with a dot (·). The residues having a $^{3}J_{HNH\alpha}$ less than 5 Hz are designated with a continuous line. The intensities of the NOEs are represented by the thickness of the lines. The values of the $\Delta^{13}C^{\alpha}$ and $\Delta^{13}C^{\beta}$ are represented by the intensity of the blocks. The secondary structure highlighting the six α-helices is indicated at the bottom of the Figure.

The structure consists of six antiparallel amphipathic α-helices, where the majority of the hydrophobic residues form an extensive network of interactions that constitute the core of the protein. The surface of the R347K TNFR-1 DD mutant is composed of several basic (R341, K343, K347, R348, R358, R365, R368, R379, R380, R381, R384, R385, R394, and R397) and several acidic (E335, E344, D353, E355, D357, E360, E369, E386, E390, D398, D400, E406, D407, E409 and E410) residues. Figure 3(a) and (c) show one face of the R347K TNFR-1 DD surface that contains an acidic patch consisting of residues from α1 (E335) and α6 (E406, D407, E409, and E410). The other face (Figure 3(b) and (d)) of the protein also contains charged residues encompassing α2 (K343, E344, and K347), the loop between α2 and α3 (R348) and part of α3 (D353). Additionally, several hydrophobic residues are surface-exposed (Y331, L340, L349, L351, L361, L367, Y372, A376, L391, M399, L402, and L412). These electrostatic patches on the surface of R347K TNFR-1 DD are suggestive of potential protein-binding sites.

Structural comparison of TNFR-1 DD mutants

Due to the poor solubility of the wild-type TNFR-1 DD, NMR structural studies were pursued on two different mutant proteins at two distinct pH values. The R347A mutant was studied at high pH (8.8), where the protein is soluble to 1 mM,[20] whereas the R347K TNFR-1 DD described herein is soluble to 1 mM at pH 4.0. The mutation in both proteins occurs in α2 and, although the solubilities

Table 1. Structural, energetic statistics, and atomic rms differences

Structural and energetic statistics	⟨SA⟩	(SA)r
rmsd from experimental distance constraints (Å) (1167)	0.0185 ± 0.001	0.0172
No. of distance constraint violations greater than 0.25Å	0	0
rmsd from experimental dihedral constraints (deg.) (92)	0.0510 ± 0.05	0.0177
No. of dihedral constraint violations greater than three (deg.)	0	0
rmsd from idealized covalent geometry		
Bonds (Å)	0.0030 ± 0.0002	0.0035
Angles (deg.)	0.409 ± 0.015	0.4410
Impropers (deg.)	0.3732 ± 0.0123	0.4327
Energetics		
E_{repel} (kcal mol^{-1}	19 ± 3	17.4
E_{NOE} (kcal mol^{-1})	20 ± 3	17.2
E_{cdih} (kcal mol^{-1})	0.03 ± 0.05	0.02
E_{bond} (kcal mol^{-1})	13.6 ± 2.5	18.6
E_{imp} (kcal mol^{-1})	15.7 ± 1	21.1
E_{ang} (kcal mol^{-1})	67.1 ± 5	78.2
Procheck[b]		
Residues in most favorable region of Ramachandran plot	93.8 ± 0.8	93.6
Residues in additionally allowed region of Ramachandran plot	5.7 ± 0.7	6.4
Residues in generously allowed region of Ramachandran plot	0.5 ± 0.2	0
Residues in disallowed region of Ramachandran plot	0	0
Overall *G*-factor	0.25 ± 0.01	0.26
No. of bad contacts	2.6 ± 1.2	3

	Non-hydrogen atomic rms differences (Å)			
	All residues[c]		Secondary structure[d]	
	Backbone atoms	All atoms	Backbone atoms	All atoms
⟨SA⟩ *versus* **SA**	0.63 ± 0.09	1.51 ± 0.11	0.40 ± 0.07	1.09 ± 0.08
⟨SA⟩ *versus* (**SA**)r	0.75 ± 0.1	1.85 ± 0.27	0.52 ± 0.07	1.38 ± 0.10
(**SA**)r *versus* **SA**	0.43	1.10	0.34	0.85

The NMR structures are denoted as follows: ⟨SA⟩ are the final 20 ensemble structures; **SA** is the mean structure obtained from averaging the Cartesian coordinates of individual ensemble members; and (**SA**)r is the minimized average structure obtained by regularization of **SA**. E_{repel} was calculated using a final force constant of 4.0 kcal mol^{-1} Å^{-4} with van der Waals hard sphere radii scaled by 0.78. E_{NOE} was calculated using a square-well potential with center-averaging and a force constant of 50 kcal mol^{-1} Å^{-2}. E_{cdih} was calculated using a force constant of 200 kcal mol^{-1} rad^{-2}. E_{bond}, E_{angle} and $E_{improper}$ were calculated using force constants of 1000 kcal mol^{-1} Å^{-2}, 500 kcal mol^{-1} rad^{-2} and 500 kcal mol^{-1} rad^{-2}, respectively.

[a] 1 cal = 4.184 J.

[b] These were calculated using the PROCHECK program.[21,22]

[c] In all atomic rms differences calculations, only the backbone atoms (N, C$^{\alpha}$ and C) are included in the least squared best fitting.

[d] Core six helices.

of the R347A and R347K TNFR-1 DD proteins are drastically different, the secondary structure in this region appears unaffected. The mutation R347K is conservative and it was somewhat surprising to find that this mutation enabled the protein to be highly soluble and stable. The structure of R347K TNFR-1 DD reveals that K347 (Figures 3(b) and 5(b)) is solvent-exposed and perhaps the mutation of R347K destabilized a network of hydrogen bond interactions crucial for self-association, therefore, stabilizing the R347K TNFR-1 DD as a monomer. Based upon this premise, it is not surprising that R347A also exists as a monomer in solution. The precise mechanism of the high solubility of R347K at pH 4.0 as compared to R347A is unclear. However, it is possible that a positively charged K347 is necessary to stabilize the monomer at pH 4.0, while A347 may cause the instability of monomer by orienting this residue toward the hydrophobic core, making it less soluble. Additionally, the pattern of inter-helical long-range NOEs (data not shown) is conserved when comparing the two TNFR-1 DD mutant proteins further supporting the observation that the structures of the two mutant proteins are essentially the same. At low concentrations (30 μM), an HSQC spectrum (data not shown) of the wild-type TNFR-1 DD collected at pH 5.0 was very consistent with the spectrum of the R347K TNFR-1 DD mutant at the same pH. These data suggest that the overall structure of R347K mutant protein determined here is similar to that of wild-type. α3 of both the R347A and R347K TNFR-1 DD mutant proteins exhibited rapid amide exchange with solvent, indicating that this α-helix is much more flexible than the other α-helices in the protein. A similar result was observed for the FADD DD[13,14] and in the crystal structure of the complex of Tube DD with the Pelle DD where the thermal parameters for α3 of the Tube DD and Pelle DD were high.[15]

Structural comparison of TNFR-1 DD with other members of the death domain superfamily

The death domain superfamily of proteins includes the death domains, the death effector

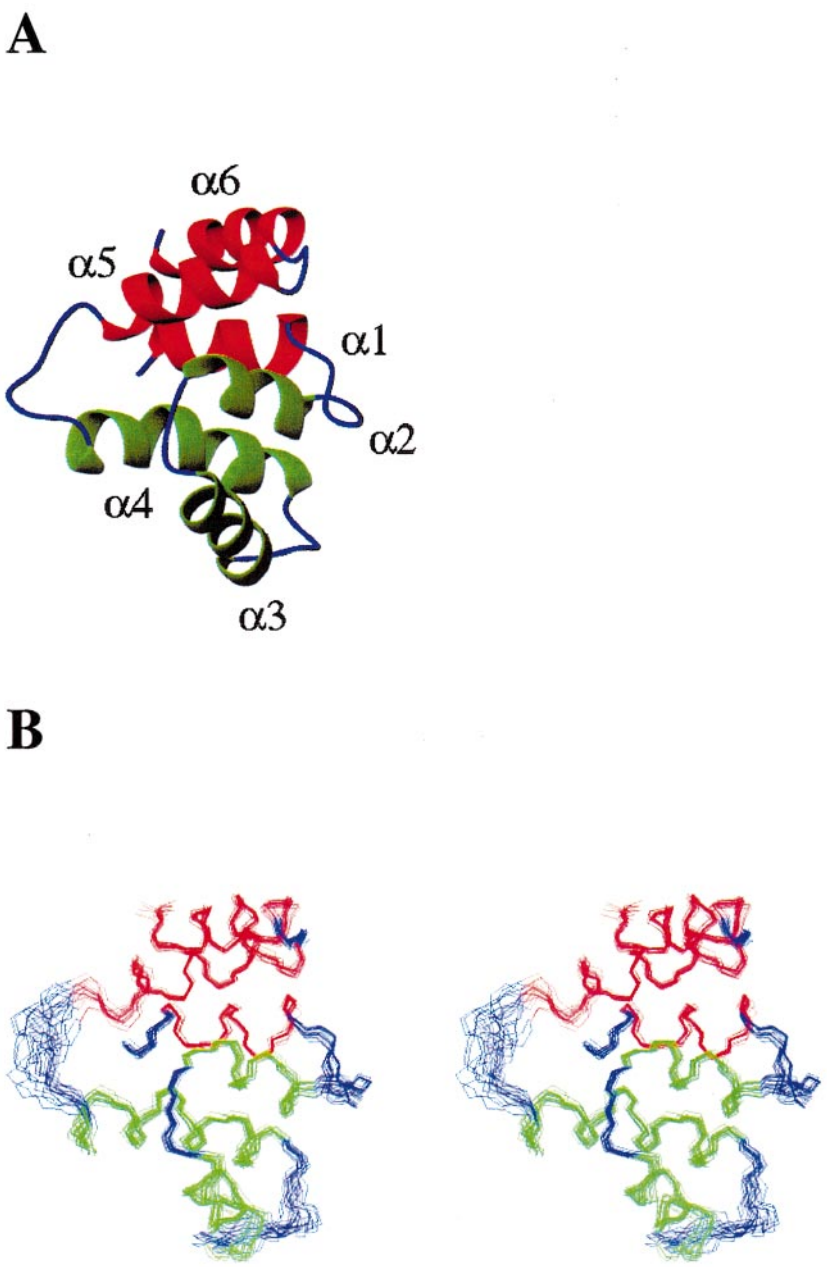

Figure 2. The solution structure of R347K TNFR-1 DD. (a) A ribbon diagram of the C^{α} trace of the averaged minimized structure of R347K TNFR-1 DD. (b) A stereoview of the superposition of the C^{α} trace of an ensemble of 20 structures calculated using the program XPLOR. No structures had distance violations >0.25 Å or angle violations >3.0°. The unstructured regions in (a) and (b) are colored in blue, while α1, α5, and α6 are colored in red and α2, α3, and α4 are colored in green.

domains, and the CARD domains, which are involved in signaling programmed cell death and homotypic interactions. Each known structure for the proteins in this superfamily contains a characteristic core of six antiparallel α-helices.[11–13,15–17,19] Typically, there is ~20% sequence identity between the various death domains[23] and less sequence homology when comparing the death domains to the death effector domains and CARD domains. All of the members in this class contain relatively short protein sequences (~100 amino acid residues) that encompass the six α-helices.

A comparison of the R347K TNFR-1 DD structure with the other known structures in the death domain superfamily has revealed that the overall fold for TNFR-1 DD is similar to the other death domains. A superposition of the six α-helical regions of R347K TNFR-1 DD with the six α-helical regions of the other proteins in the death domain superfamily was performed utilizing the program DEJAVU.[24] The observed deviations when comparing the R347K TNFR-1 DD structure to the other protein structures in the death domain superfamily reside in either helix length or helix orientation (Figure 4). A detailed analysis of the death domain structures revealed that the structures of p75 neurotrophin and the Pelle DD were the most similar to TNFR-1 DD having a rmsd of 1.82 Å and 2.09 Å for 69 C^{α} atoms composed of the α-helical core, respectively. The similarity to TNFR-1 DD is followed by the Tube DD, Fas DD, and FADD DD having rmsds of 2.15 Å, 2.28 Å, and 2.27 Å for the

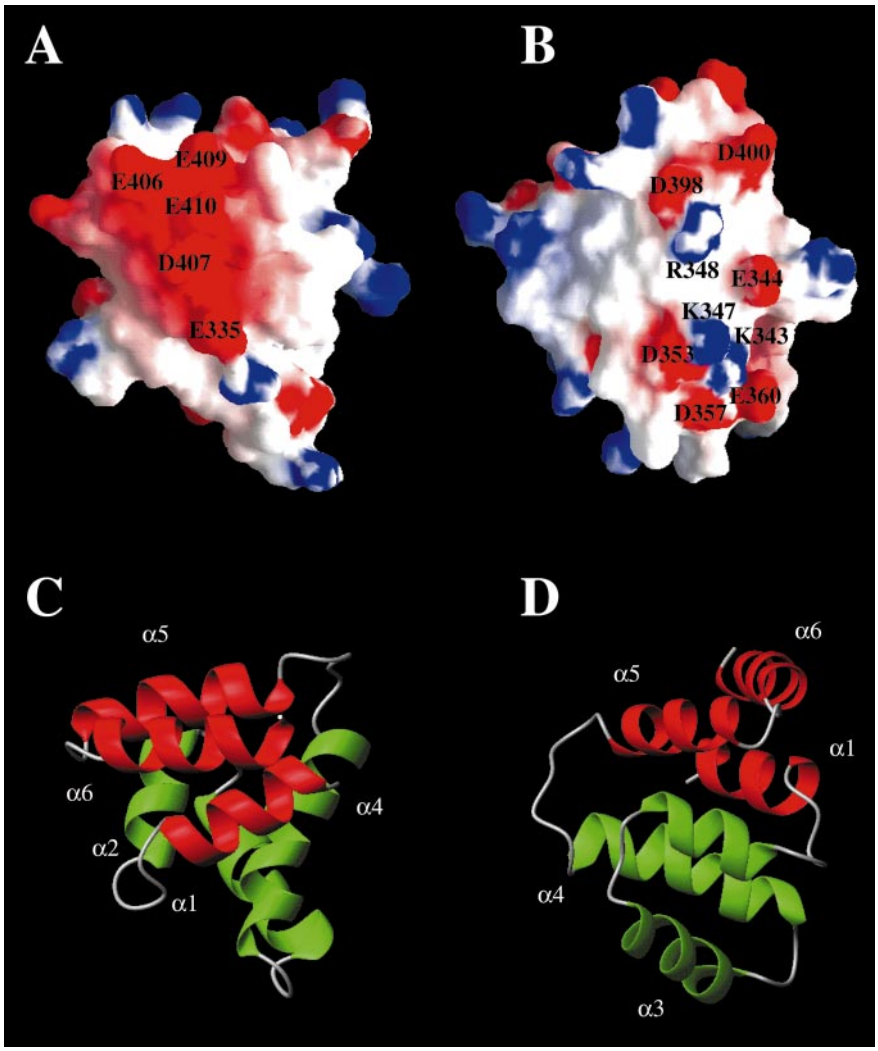

Figure 3. Surface diagram of R347K TNFR-1 DD. The surface electrostatic potential in (a) and (b) is color-coded such that regions of the surface that are negatively charged are colored in red and regions that are positively charged are colored in blue. (c) and (d) Ribbon diagrams of the C^{α} trace of the averaged minimized structure of R347K TNFR-1 DD displaying the orientations depicted in (a) and (b), respectively. For clarity, α1, α5, and α6 are colored in red and α2, α3, and α4 are colored in green.

65 C^{α}, 69 C^{α}, and 57 C^{α} atoms in the α-helical core, respectively. Comparison of TNFR-1 DD with the CARD domains resulted in rmsds of 1.85 Å, 2.19 Å, and 1.95 Å for the 43 C^{α}, 62 C^{α}, and 60 C^{α} atoms in the core α-helical region for the RAIDD CARD, Apaf-1 CARD, and procaspase-9 structures, respectively. Overlay of R347K TNFR-1 DD mutant with the FADD DED resulted in rmsds of 2.12 Å for the 55 C^{α} atoms in the α-helical regions of FADD DED and Tube DD, respectively.

Discussion

Although the structural overlay of R347K TNFR-1 DD with the other proteins in the death domain superfamily yielded reasonable rmsd values, consistent with the similarity in the overall folds, the major structural difference between R347K TNFR-1 DD and the other death domain-like proteins resides in the relative orientations of α2, α3, and α4. In the R347K TNFR-1 DD solution structure, α2 and α4 are aligned parallel with one another and the orientation of α3 is almost perpendicular to α2 and α4. P75 neurotrophin and the Pelle DD are the only members of the death domain superfamily that retain the same relative orientation of α2, α3, and α4 as R347K TNFR-1 DD. The lengths of α2 and α3 are very similar among all the family members; however, α4 of Fas DD,[11] p75 neurotrophin,[12] and FADD DED[16] are much shorter (consisting of 11, ten, and seven residues, respectively) than the length of α4 (13 residues) for R347K TNFR1-DD. Additionally, the length of α1 of R347K TNFR-1 DD consisting of eight residues is much shorter than α1 of the FADD DD (14 residues),[13,14] the RAIDD CARD domain (13 residues),[17] and Apaf-1 CARD (12 residues).[18] The observed differences, including helical length and orientation of the

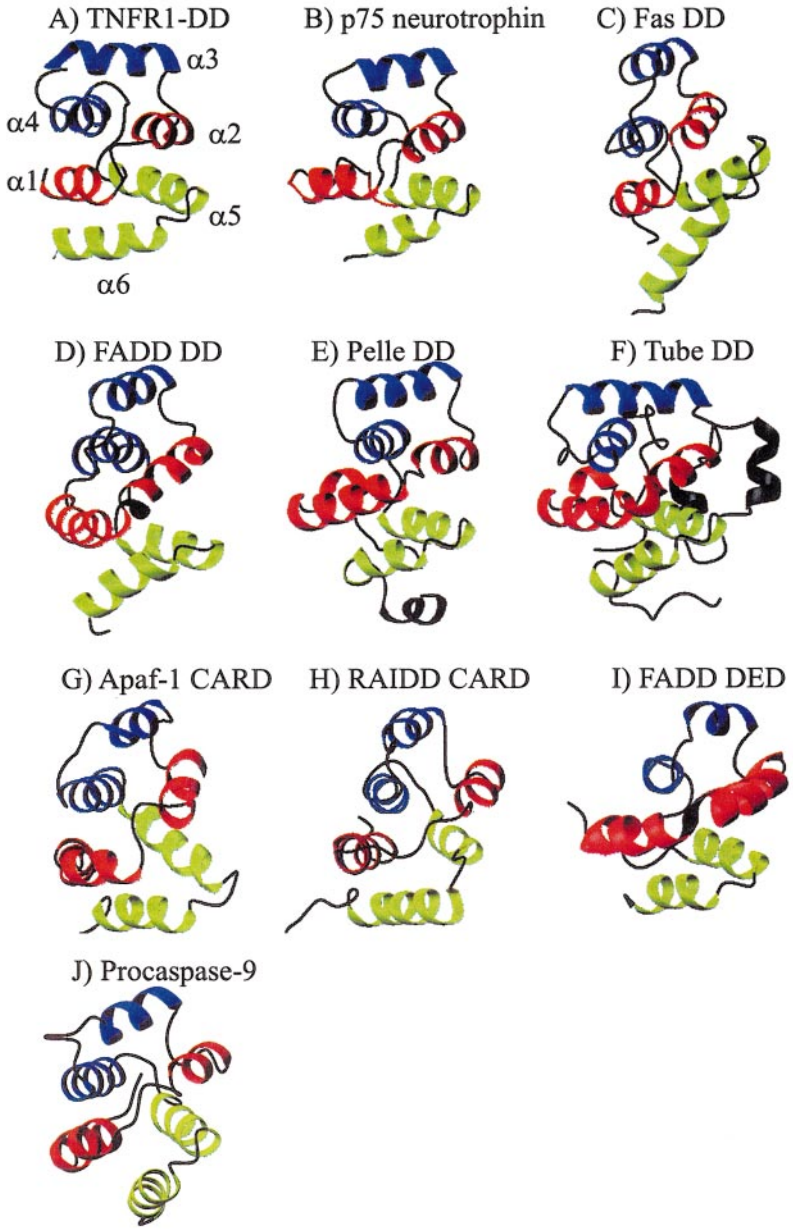

Figure 4. Ribbon diagram of proteins in the death domain superfamily. The orientation of each protein in the death domain superfamily is shown based upon the best superposition with R347K TNFR-1 DD. For clarity, α1 and α2 are colored red, α3 and α4 are colored blue, and α5 and α6 are colored green. The pdb files utilized are indicated below: (a) R347K TNFR-1 DD, (b) p75 neurotrophin (1ngr.pdb),[12] (c) Fas DD (1ddf.pdb),[11] (d) FADD DD (1fad.pdb),[13] (e) Pelle DD (1d2z.pdb),[15] (f) Tube DD (1d2z.pdb),[15] (g)Apaf-1 CARD (1c15.pdb),[18] (h) RAIDD CARD (3crd.pdb),[17] (i) FADD DED (1a1z.pdb),[16] and (j) Procaspase-9 (3ygs.pdb).[19]

members in the death domain superfamily with respect to the R347K TNFR-1 DD solution structure, are summarized in Figure 4.

Several of the proteins in the death domain superfamily, including Fas DD,[11] RAIDD CARD,[17] and the FADD DD,[13,14], have charged surfaces and it is presumed that electrostatic interactions are the driving force for homotypic interactions. Recently, crystal structures of complexes formed between procaspase-9 with APAF-1 CARD[19] and the Pelle DD with the Tube DD[15] have shown that the surfaces involved in the homotypic interactions are charged and of opposite polarity. Nevertheless, the mode of interaction in both cases was driven by a network of hydrogen bond contacts as well as by van der Waals interactions instead of electrostatic interactions as suggested by the protein surface. In the case of TNFR-1 DD, it was recently shown that the interaction between TNFR-1 DD and TRADD DD could be disrupted by salt.[20] This is consistent with the molecular surface for the solution structure of the R347K TNFR-1 DD mutant, which contains several charged residues including an acidic patch (Figure 3(a)) on one face of the protein and

several basic residues on the other face of the protein (Figure 3(b)). Several of the charged residues are located in α2 and α3, which correlates well with the identified self-association and protein association sites on TNFR-1 DD,[20] Fas DD[11] and FADD DD.[13,14] These observations suggest that the mode of interaction of TNFR-1 DD with TRADD DD may be primarily electrostatic in nature.

Mutagenesis studies[20] have shown that α2 and part of α3 and α4 contain important residues for both self-association and interaction with the TRADD DD. As described previously, these regions of the TNFR-1 DD protein are also correlated with surface-exposed charged residues (Figure 5(a) and (b)). The mutants that affect both self-association and interaction with the TRADD DD are located on two distinct faces of the protein. One face contains critical residues from α2 and part of α3 (K343A, E344A, R347A, R348A, and D353A) where these residues are colored yellow in Figure 5(b). This is consistent with the previous observation that the surface formed by α2 and α3 has been implicated in the homo and hetero-association of the death domains of Fas[11] and FADD.[13,14] However, a major structural difference is observed when comparing the orientations of α2, α3, and α4 of Fas DD and FADD DD with TNFR-1 DD. The orientation of α3 in TNFR1-DD is nearly perpendicular to α2 and α4, whereas in the Fas DD and FADD DD structures α3 is aligned antiparallel to α2 and α4. The observed structural differences in α3 correlates well with the differences in the contribution of this helix to their binding properties, based upon site-directed mutagenesis studies of TNFR1-DD[20] and Fas DD.[11] Fas DD appears to rely more on α3 for its interaction than TNFR1-DD does, as four out of four mutations in this helix completely abolish the self-association of Fas DD, while only one corresponding mutation (D353) in TNFR-1 DD has a similar effect. A 180° rotation

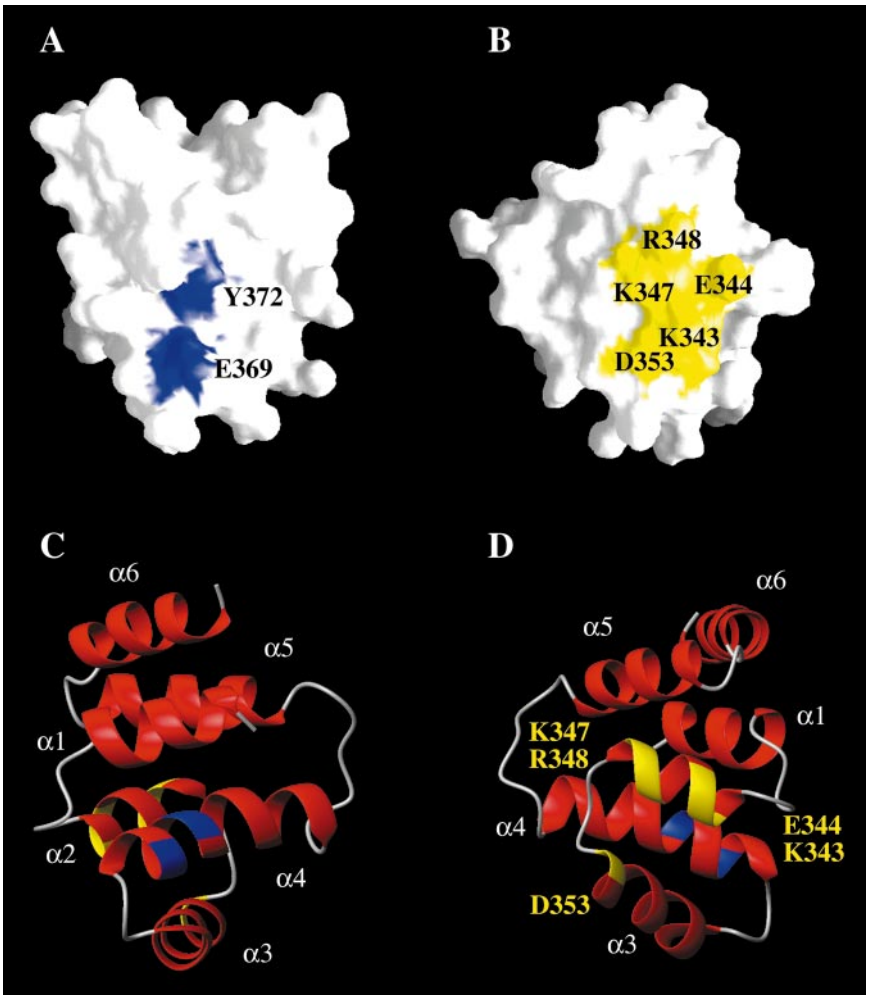

Figure 5. (a) and (b) Surface diagrams displaying distinct orientations of R347K TNFR1-DD. Mutated residues that disrupt self-association and binding to TRADD DD[20] are colored blue in (a) and yellow in (b). (c) and (d) Ribbon diagrams of the C^{α} trace of the averaged minimized structure of R347K TNFR-1 DD displaying the orientations depicted in (a) and (b), respectively. In (c) and (d), the α-helical regions are colored red, the loop regions are colored gray, and the mutated residues that disrupt self-association and binding to TRADD DD are colored in blue and yellow.

highlights the other surface composed of key residues in α4 (E369A and Y372F) (Figure 5(a)). A similar result was seen for the complex structure of the Tube and Pelle death domains, where α4 and α5 of the Pelle death domain interacts with α6 and the unique C-terminal tail of the Tube death domain.[15] These results imply that, despite the similarity in the interaction surfaces for death domains, a substantial difference can exist.

The observation that mutations in two distinct surfaces of TNRF-1 DD disrupts both self-association and interaction with the TRADD DD is consistent with the proposed mechanism of TNFR-1 DD activity.[4] Since ligand-induced TNFR-1 trimer formation is a prerequisite step for the recruitment of TRADD to the cell surface, it is possible that this is due to the requirement of the trimerization of TNFR-1 DD for interacting with TRADD DD. Therefore, the two surfaces identified on TNFR-1 DD by site-directed mutagenesis may simply correspond to the self-association binding sites but not the TRADD interaction sites.[20] Indeed, all the mutations that abolish the ability to interact with TRADD DD also fail to self-associate, supporting this model. Nevertheless, it is still plausible that the TRADD DD binding site overlaps with the TNFR-1 DD self-association site, especially given that a unique TRADD DD binding site has not been identified. If this is the case, the ligand-induced trimerization of the receptor may simply expose the interaction site in TNFR1-DD by releasing a negative regulator, such as SODD silencer of death domains (SODD).[25] It is worth mentioning that, in the case of the Fas[11] and FADD[13,14] death domains, mutagenesis data identified distinct residues associated with homo and hetero-interactions, implying a potential difference between the binding properties of TNFR-1 DD and FAS DD.

The surface of the R347K TNFR-1 DD structure also contains an acidic patch (Figure 3(a)) consisting of residues from α1 and α6, but mutation of E406A and E410A (of α6) had no effect on self-association or binding to TRADD DD.[20] The assembly of the TNFR-1 DD trimer may present this acidic patch as a potential binding site for an undetermined death domain in another signaling cascade. Additionally, the acidic patch on TNFR-1 DD may represent the binding site of a negative regulatory protein, such as SODD,[25] of TNFR-1 activity that is potentially released upon trimer formation. A potential functional role for α6 in TNFR-1 DD would be consistent with the observed result from the crystal structure of the complex between the Tube DD and Pelle DD, where α6 from the Tube death domain comprises part of the interaction site.[15]

The comparison of TNFR-1 DD with the other members of the death domain superfamily of proteins revealed that the major difference in the structures relative to TNFR-1 DD resides in the lengths and orientation of α2, α3, or α4. The location of the structural change between the death domains is consistent with mutagenesis studies that have identified critical residues for both self-association and binding to TRADD DD in these regions of the protein.[20] Particularly, the mutagenesis data identify the two putative self-association binding sites for TNFR-1 DD. One site is consistent with the identification of the homo-binding sites for Fas DD[11] and FADD DD.[13,14] Despite the similarity in the overall fold, the observed differences in the local structure and sequence between TNFR-1 DD and the other proteins in the death domain superfamily correlate with the functional regions of the proteins. This may account for the selectivity of signaling cascade initiated from TNFR-1. The observations that the nature of the protein-protein interaction can vary greatly further supports the apparent versatile nature of the death domain fold.

Materials and Methods

TNFR-DD cloning and site-directed mutagenesis (R347K TNFR-1 DD)

The DNA sequence coding from amino acid residues 316-426 from hTNFR-1 was cloned in pRSETB (Invitrogen) after amplification by PCR. The primer at the 5′ end introduces an initiation site with an *Nde*I site upstream of the methionine residue, and the primer at the 3′ end introduces a His tag after amino acid residue 426. The sequence was confirmed by sequencing analysis. A single-point mutation (R347K) was introduced using chameleon double-stranded site-directed mutagenesis (Stratagene) and verified by sequencing of the coding region.

Protein expression

R347K TNFR-1 DD protein was overexpressed in BL-21 *Escherichia coli*. Cells were grown at 25 °C on minimal medium containing either 2 g l^{-1} [^{15}N]ammonium sulfate or [^{15}N]ammonium sulfate and 2 g l^{-1} ^{13}C glucose. The cells were then lysed and R347K TNFR-1 DD mutant protein was purified (see below).

Purification of R347K TNFR-1 DD protein

Twenty grams of wet cell paste expressing R347K TNFR-1 DD were resuspended in 300 ml of lysis buffer containing 50 mM Tris-HCl (pH 7.5), 50 mM NaCl, and protease inhibitor tablets (Boehringer Mannheim GmbH, Mannheim, Germany). Cells were lysed by two passages through a Microfluidizer (Microfluidics Corporation, Newton, MA). The cell lysate was centrifuged at 15,000 ***g*** for 30 minutes. The TNFR-1 DD protein was then extracted from the pellet with 200 ml of pH 8.8 buffer (50 mM Tris, (pH(8.8) and 50 mM NaCl). The extraction was performed three times until no additional protein was solubilized. Then 40 ml of Ni-NTA resin (Qiagen) was added to the combined extract. The resin was first washed with pH 8.8 buffer followed by pH 8.8 buffer containing 50 mM imidazole. The R347K TNFR-1 DD protein was then eluted with 400 mM imidazole in pH 8.8 buffer. DTT was added immediately to the eluate to a final concentration of 10 mM. The eluted protein was pooled and dialyzed against buffer containing 50 mM sodium acetate (pH 4.0-4.2) and 10 mM DTT overnight. The protein was then concentrated using a Centriprep (YM-10, Amicon) to about 6 mg ml^{-1} and applied to G3000SW (TOSOHASS) column pre-

equilibrated with 10 mM sodium acetate (pH 4.0) and 10 mM DTT. The monomeric fraction was pooled and concentrated for NMR studies.

NMR data collection, complete assignments and secondary structure determination

All spectra were recorded at 35 °C on a Varian Unity Plus 600 spectrometer equipped with a triple-resonance $^{1}H/^{13}C/^{15}N$ probe and an actively shielded *z*-gradient pulsed field accessory. ^{1}H-^{15}N HSQC and all HSQC-based ^{15}N edited 3D experiments on ^{15}N-labeled and triple-resonance 3D experiments on $^{15}N/^{13}C$ double-labeled protein were recorded with the enhanced-sensitivity pulsed field gradient approach.[26] This approach provides coherence transfer selection both to improve sensitivity and to eliminate artifacts as well as for solvent suppression. The complete assignments (>95 %) of the ^{1}H, ^{15}N and ^{13}C resonances are summarized in the Supplementary Material (Table 1S) and were based on the following experiments: CBCA(CO)NNH,[27] HNCACB,[28] C(CC)TOCSY_NNH,[29] H(CC)TOCSY_NNH,[29] HBHA(CBCACO)NNH.[30] 2D ^{13}C (methyl)-^{1}H HSQC and methyl relay experiments were used for auxiliary methyl assignments of valine, leucine and isoleucine residues.[31,32] Some ambiguous resonances were further confirmed by analysis of the simultaneous $^{15}N/^{13}C$-edited NOESY[33] experiment. R347K TNFR-1 DD is a proline-rich protein, which contains several peptidyl-prolyl (*cis*/*trans*) isomers. Most of the proline residues were detected using a new experiment that connects sequential residues *via* their ^{15}N nuclei.[34] The 4D ^{13}C, ^{13}C-edited NOESY[35] were carried out on a double-labeled ($^{15}N/^{13}C$) sample in $^{2}H_2O$ to assign overlapped γ-methyl groups of valine and the δ-methyl groups of leucine and isoleucine residues and also to identify some long-range NOEs between these methyl groups. Data sets were typically processed and displayed on an SGI workstation using the NMRDraw and NMRPipe[36] programs. A skewed 60° phase-shifted sine-bell function and a single zero-filling were used in each of the three dimensions prior to Fourier transformation. For triple-resonance 3D experiments, the time domain was extended by a factor of 2 using forward-backward linear prediction in the ^{15}N (*t*2) dimension. For constant-time ^{1}H-^{13}C correlation experiments, mirror image linear prediction was used prior to zero-filling to double the time domain data points.[37] The programs PIPP and STAPP[38] were used for data analysis and semi-automatic assignments.[37]

The secondary structure of R347K TNFR-1 DD was based on characteristic NOEs involving the amide NH, H^{α}, and H^{β} protons from ^{15}N-edited NOESY and simultaneous $^{15}N/^{13}C$-edited NOESY spectra, three-bond *J*-coupling constants ($^{3}J_{HNH\alpha}$) from the 3D HNHA, slowly exchanging amide protons with $^{2}H_2O$, and C^{α} and C^{β} secondary chemical shifts. It was determined that the secondary structure of R347K TNFR-1 DD is composed of six α-helices, ranging in length from seven to 13 residues. α3 (residues D353-L361) appears to be more flexible, as evident by the increased amide exchange rates relative to other α-helical regions in the protein.

R347K TNFR-1 DD structure calculation

The solution structure is based on inter-proton distance constraints converted from observed NOEs in both the ^{15}N-edited NOESY[39,40] and simultaneous $^{15}N/^{13}C$-edited NOESY experiments. The NOEs were classified as either strong (1.8-2.7 Å), medium (1.8-3.3 Å) or weak (1.8-5.5 Å) constraints. Upper distance limits for NOEs involving methyl protons and non-stereospecifically assigned methylene protons were corrected appropriately for center averaging,[41] and an additional 0.5 Å was added to upper distance limits for NOEs involving methyl protons.[42,43] φ and ψ torsion angle constraints were obtained from the 3D HNHA experiment[44] and from ^{15}N, H^{α}, C^{α}, and C^{β} chemical shifts using the TALOS[45] program.

The structures were calculated using the hybrid distance geometry-dynamical simulated annealing method of Nilges *et al*.[46] with minor modifications[47] using the program XPLOR,[48] adapted to incorporate pseudopotential secondary C^{α}/C^{β} chemical shift constraints[49] and a conformational database potential.[50,51] The target function that is minimized during restrained minimization and simulated annealing comprises only quadratic harmonic terms for covalent geometry and secondary C^{α}/C^{β} chemical shift constraints, square-well quadratic potentials for the experimental distance and torsion angle constraints, and a quartic van der Waals term for non-bonded contacts. All peptide bonds were constrained to be planar and *trans*. There were no hydrogen-bonding, electrostatic, or 6-12 Lennard-Jones empirical potential energy terms in the target function.

Protein Data Bank accession numbers

The coordinates have been deposited, with the PDB identification code 1ICH. They have also been deposited at the Research Collaboratory for Structural Bioinformatics (RCSB), with the identification code RCSB013155.

Acknowledgments

We thank Dr Mark Stahl, Dr Jean-Baptiste Telliez, and Dr John Woronicz for all of the valuable insight provided on this project.

References

1. Tartaglia, L. A. & Goeddel, D. V. (1992). Two TNF receptors. *Immunol. Today*, **13**, 151-153.
2. Grell, M., Scheurich, P., Meager, A. & Pfizenmaier, K. (1993). TR60 and TR80 tumor necrosis factor (TNF)-receptors can independently mediate cytolysis. *Lymphokine Cytokine Res.* **12**, 143-148.
3. Tartaglia, L. A., Rothe, M., Hu, Y. F. & Goeddel, D. V. (1993). Tumor necrosis factor's cytotoxic activity is signaled by the p55 TNF receptor. *Cell*, **73**, 213-216.
4. Smith, C. A., Farrah, T. & Goodwin, R. G. (1994). The TNF receptor superfamily of cellular and viral proteins: activation, costimulation, and death. *Cell*, **76**, 959-962.
5. Hsu, H., Xiong, J. & Goeddel, D. V. (1995). The TNF receptor 1-associated protein TRADD signals cell death and NF-kappa B activation. *Cell*, **81**, 495-504.
6. Hsu, H., Shu, H. B., Pan, M. G. & Goeddel, D. V. (1996). TRADD-TRAF2 and TRADD-FADD interactions define two distinct TNF receptor 1 signal transduction pathways. *Cell*, **84**, 299-308.
7. Hsu, H., Huang, J., Shu, H. B., Baichwal, V. & Goeddel, D. V. (1996). TNF-dependent recruitment

of the protein kinase RIP to the TNF receptor- 1-signaling complex. *Immunity,* **4**, 387-396.
8. Boldin, M. P., Mett, I. L., Varfolomeev, E. E., Chumakov, I., Shemer-Avni, Y., Camonis, J. H. & Wallach, D. (1995). Self-association of the ''death domains'' of the p55 tumor necrosis factor (TNF) receptor and Fas/APO1 prompts signaling for TNF and Fas/APO1 effects. *J. Biol. Chem.* **270**, 387-391.
9. Tartaglia, L. A., Ayres, T. M., Wong, G. H. W. & Goeddel, D. V. (1993). A novel domain within the 55 kd TNF receptor signals cell death. *Cell,* **74**, 845-853.
10. Itoh, N. & Nagata, S. (1993). A novel protein domain required for apoptosis. Mutational analysis of human Fas antigen. *J. Biol. Chem.* **268**, 10932-10937.
11. Huang, B., Eberstadt, M., Olejniczak, E. T., Meadows, R. P. & Fesik, S. W. (1996). NMR structure and mutagenesis of the Fas (APO-1/CD95) death domain. *Nature,* **384**, 638-641.
12. Liepinsh, E., Ilag, L. L., Otting, G. & Ibanez, C. (1997). NMR structure of the death domain of the p75 neurotrophin receptor. *EMBO J.* **16**, 4999-5005.
13. Jeong, E.-J., Bang, S., Lee, T. H., Park, Y. I., Sim, W.-S. & Kim, K.-S. (1999). The solution structure of FADD death domain. *J. Biol. Chem.* **274**, 16337-16342.
14. Berglund, H., Olerenshaw, D., Sankar, A., Federwisch, M., McDonald, N. Q. & Driscoll, P. C. (2000). The three-dimensional solution structure and dynamic properties of the human FADD death domain. *J. Mol. Biol.* **302**, 171-188.
15. Xiao, T., Towb, P., Wasserman, S. A. & Sprang, S. R. (1999). Three-dimensional structure of a complex between the death domains of pelle and tube. *Cell,* **99**, 545-555.
16. Eberstadt, M., Huang, B., Chen, Z., Meadows, R. P., Ng, S. C. & Zheng, L. *et al*. (1998). NMR structure and mutagenesis of the FADD (Mort1) death-effector domain. *Nature,* **392**, 941-945.
17. Chou, J. J., Matsuo, H., Duan, H. & Wagner, G. (1998). Solution structure of the RAIDD CARD and model for CARD/CARD interaction in caspase-2 and caspase-9 recruitment. *Cell,* **94**, 171-180.
18. Zhou, P., Chou, J., Olea, R. S., Yuan, J. & Wagner, G. (1999). Solution structure of Apaf-1 CARD and its interaction with caspase-9 CARD: a structural basis for specific adaptor/caspase interaction. *Proc. Natl Acad. Sci. USA,* **96**, 11265-11270.
19. Qin, H., Srinivasula, S. M., Wu, G., Fernandes-Alnemri, T., Alnemri, E. S. & Shi, Y. (1999). Structural basis of procaspase-9 recruitment by the apoptotic protease-activating factor1. *Nature,* **399**, 549-557.
20. Telliez, J. B., Xu, G. Y., Woronicz, J. D., Hsu, S., Wu, J. L. & Lin, L. *et al*. (2000). Mutational analysis and NMR studies of the death domain of the tumor necrosis factor receptor-1. *J. Mol. Biol.* **300**, 1323-1333.
21. Laskowski, R. A., MacArthur, M. W., Moss, D. S. & Thornton, J. M. (1993). PROCHECK: a program to check the stereochemical quality of protein structures. *J. Appl. Crystallog.* **26**, 283-291.
22. Laskowski, R. A., Rullmannn, J. A., MacArthur, M. W., Kaptein, R. & Thornton, J. M. (1996). AQUA and PROCHECK-NMR: programs for checking the quality of protein structures solved by NMR. *J. Biomol. NMR,* **8**, 477-486.
23. Feinstein, E., Kimchi, A., Wallach, D., Boldin, M. & Varfolomee, E. (1995). The death domain: a module shared by proteins with diverse cellular functions. *Trends Biochem. Sci.* **20**, 342-344.
24. Kleywegt, G. J. & Jones, T. A. (1999). Detecting folding motifs and similarities. *Methods. Enzymol.* **277**, 525-545.
25. Jiang, Y., Woronicz, J. D., Liu, W. & Goeddel, D. V. (1999). Prevention of constitutive TNF receptor 1 signaling by silencer of death domains. *Science,* **283**, 543-546.
26. Kay, L. E. (1995). Pulsed field gradient multi-dimensional NMR methods for the study of protein structure and dynamics in solution. *Prog. Biophys. Mol. Biol.* **63**, 277-299.
27. Grzesiek, S. & Bax, A. (1992). Correlating backbone amide and side-chain resonances in larger proteins by multiple relayed triple resonance NMR. *J. Am. Chem. Soc.* **114**, 6291-6293.
28. Muhandiram, D. R. & Kay, L. E. (1994). Gradient enhanced triple-resonance three dimensional NMR experiments with improved sensitivity. *J. Magn. Reson.* **103**, 203-216.
29. Grzesiek, S., Anglister, J. & Bax, A. (1993). Correlation of backbone amide and aliphatic side-chain resonances in $^{13}C/^{15}N$-enriched proteins by isotropic mixing of carbon-13 magnetization. *J. Magn. Reson. ser. B,* **101**, 114-119.
30. Grzesiek, S. & Bax, A. (1993). Amino acid type determination in the sequential assignment procedure of uniformity carbon-13/nitrogen-15-enriched proteins. *J. Biomol. NMR,* **3**, 185-204.
31. Bax, A., Max, D. & Zax, D. (1992). Measurement of long-range ^{13}C-^{13}C J couplings in a 20-kDa protein-peptide complex. *J. Am. Chem. Soc.* **114**, 6923-6925.
32. Grzesiek, S., Vuister, G. W. & Bax, A. (1993). A simple and sensitive experiment for measurement of J_{CC} couplings between backbone carbonyl and methyl carbons in isotopically enriched proteins. *J. Biomol. NMR,* **3**, 487-493.
33. Pascal, S. M., Muhandiram, D. R., Yamazaki, T., Forman-Kay, J. D. & Kay, L. E. (1994). Nuclear magnetic resonance structure of an SH2 domain of phospholipase C-gamma 1 complexed with a high affinity binding peptide. *J. Magn. Reson.* **103**, 197-201.
34. Kanelis, V., Farrow, N. A., Kay, L. E., Rotin, D. & Forman-Kay, J. D. (1998). NMR studies of tandem WW domains of Nedd4 in complex with a PY motif-containing region of the epithelial sodium channel. *Biochem. Cell Biol.* **76**, 341-350.
35. Xu, G. Y., Ong, E., Gilkes, N. R., Kilburn, D. G., Muhandiram, D. R. & Harris-Brandts, M. *et al*. (1995). Solution structure of a cellulose-binding domain from Cellulomonas fimi by nuclear magnetic resonance spectroscopy. *Biochemistry,* **34**, 6993-7003.
36. Delaglio, F., Grzesiek, S., Vuister, G. W., Zhu, G., Pfeifer, J. & Bax, A. (1995). NMRPipe: a multidimensional spectral processing system based on UNIX pipes. *J. Biomol. NMR,* **6**, 277-293.
37. Zhu, G. & Bax, A. (1992). Improved linear prediction of damped NMR signals using modified ''forward-backward'' linear prediction. *J. Magn. Reson.* **100**, 202-207.
38. Garrett, D. S., Powers, R., Gronenborn, A. M. & Clore, G. M. (1991). A common sense approach to peak picking in two-, three-, and four-dimensional

spectra using automatic computer analysis of contour diagrams. *J. Magn. Reson.* **95**, 214-220.
39. Marion, D., Driscoll, P. C., Kay, L. E., Wingfield, P. T., Bax, A., Gronenborn, A. M. & Clore, G. M. (1989). Overcoming the overlap problem in the assignment of ^{1}H NMR spectra of larger proteins by use of three-dimensional heteronuclear ^{1}H-^{15}N Hartmann-Hahn-multiple quantum coherence and nuclear Overhauser-multiple quantum coherence spectroscopy: application to interleukin 1 beta. *Biochemistry,* **28**, 6150-6156.
40. Zuiderweg, E. R. & Fesik, S. W. (1989). Heteronuclear three-dimensional NMR spectroscopy of the inflammatory protein C5a. *Biochemistry,* **28**, 2387-2391.
41. Wuthrich, K., Billeter, M. & Braun, W. (1983). Pseudo-structures for the 20 common amino acids for use in studies of protein conformations by measurements of intramolecular proton-proton distance constraints with nuclear magnetic resonance. *J. Mol. Biol.* **169**, 949-961.
42. Clore, G. M., Gronenborn, A. M., Nilges, M. & Ryan, C. A. (1987). Three-dimensional structure of potato carboxypeptidase inhibitor in solution. A study using nuclear magnetic resonance, distance geometry, and restrained molecular dynamics. *Biochemistry,* **26**, 8012-8023.
43. Wagner, G., Braun, W., Havel, T. F., Schaumann, T., Go, N. & Wuthrich, K. (1987). Protein structures in solution by nuclear magnetic resonance and distance geometry. The polypeptide fold of the basic pancreatic trypsin inhibitor determined using two different algorithms, DISGEO and DISMAN. *J. Mol. Biol.* **196**, 611-639.
44. Garrett, D. S., Kuszewski, J., Hancoca, T. J., Lodi, P. J., Vuister, G. W., Gronenborn, A. M. & Clore, G. M. (1994). The impact of direct refinement against three-bond HN-C$^{\alpha}$H coupling constants on protein structure determination by NMR. *J. Magn. Reson.* **104**, 99-103.
45. Cornilescu, G., Delaglio, F. & Bax, A. (1999). Protein backbone angle restraints from searching a database for chemical shift and sequence homology. *J. Biomol. NMR,* **13**, 289-302.
46. Nilges, M., Gronenborn, A. M., Brunger, A. T. & Clore, G. M. (1988). Determination of three-dimensional structures of proteins by simulated annealing with interproton distance restraints. Application to crambin, potato carboxypeptidase inhibitor and barley serine proteinase inhibitor 2. *Protein Eng.* **2**, 27-38.
47. Clore, G. M., Appella, E., Yamada, M., Matsushima, K. & Gronenborn, A. M. (1990). Three-dimensional structure of interleukin 8 in solution. *Biochemistry,* **29**, 1689-1696.
48. Brunger, A. T. (1993). *X-PLOR Version 3.1 Manual,* Yale University, New Haven CT.
49. Kuszewski, J., Qin, J., Gronenborn, A. M. & Clore, G. M. (1995). The impact of direct refinement against ^{13}C alpha and ^{13}C beta chemical shifts on protein structure determination by NMR. *J. Magn. Reson. ser. B,* **106**, 92-96.
50. Kuszewski, J., Gronenborn, A. M. & Clore, G. M. (1996). Improving the quality of NMR and crystallographic protein structures by means of a conformational database potential derived from structure databases. *Protein Sci.* **5**, 1067-1080.
51. Kuszewski, J., Gronenborn, A. M. & Clore, G. M. (1997). Improvements and extensions in the conformational database potential for the refinement of NMR and X-ray structures of proteins and nucleic acids. *J. Magn. Reson.* **125**, 171-177.

Edited by P. E. Wright

(Received 1 February 2001; received in revised form 9 May 2001; accepted 15 May 2001)

http://www.academicpress.com/jmb

Supplementary Material for this paper comprising one Table is available on IDEAL